Identification of an ambisense kolmiovirus from birds

Mai Kishimoto[1,2,3,*], Sakiho Imai[3], Manabu Igarashi[4,5], Masayuki Horie[1,2,3,*]

[1] Laboratory of Veterinary Microbiology, Graduate School of Veterinary Science, Osaka Metropolitan University, Izumisano, Osaka, Japan

[2] Osaka International Research Center for Infectious Diseases, Osaka Metropolitan University, Osaka, Japan

[3] School of Veterinary Science, College of Life, Environment, and Advanced Science, Osaka Prefecture University, Izumisano, Osaka, Japan

[4] Division of Global Epidemiology, International Institute for Zoonosis Control, Hokkaido University, Sapporo, Hokkaido, Japan

[5] International Collaboration Unit, International Institute for Zoonosis Control, Hokkaido University, Sapporo, Hokkaido, Japan

[*]Corresponding authors

Mai Kishimoto, DVM, PhD

Laboratory of Veterinary Microbiology, Graduate School of Veterinary Science, Osaka Metropolitan University, 1-58 Rinku Orai-kita, Izumisano 598-8531, Osaka, Japan

Email: m.kishimoto@omu.ac.jp

Masayuki Horie, DVM, PhD

Laboratory of Veterinary Microbiology, Graduate School of Veterinary Science, Osaka Metropolitan University, 1-58 Rinku Orai-kita, Izumisano 598-8531, Osaka, Japan

E-mail: mhorie@omu.ac.jp

Abstract

Viruses in the family *Kolmioviridae* (KoVs) are unique among RNA viruses in that they have small, highly self-complementary, circular, negative-sense genomes and are satellite viruses requiring the envelope protein of co-infected helper viruses to form infectious virions. For approximately 40 years, only hepatitis D virus (HDV) had been identified, but recent studies have uncovered novel KoVs in diverse animal species. Serinus canaria-associated deltavirus (scKoV) was recently identified form a single RNA-seq data from canary skin. However, only the partial genome sequence corresponding to the transcript encoding DAg has been identified, leaving questions regarding its full genetic composition and origins. In this study, we examined publicly available RNA-seq data and identified multiple complete genome sequences of scKoV. Our results demonstrated that genetically diverse scKoVs infect multiple bird species with recent inter-order transmission. Additionally, scKoV was detected in various tissues including parenchymal organs, suggesting that scKoV is a genuine avian KoV. Notably, analysis of the genome structure and transcriptional pattern clearly revealed that scKoV transcribes a genomic-sense mRNA encoding a novel gene, in addition to the previously known antigenomic-sense DAg transcript. Furthermore, this newly identified gene appears to express two protein isoforms via alternative splicing. These findings mark the first KoV with an ambisense genome that utilizes alternative splicing, which may represent a strategy to increase gene-coding capacity despite the constraints imposed by its small and self-complementarity genome. Moreover, co-infection with avian bornaviruses was detected in most scKoV-positive RNA-seq datasets, suggesting that avian bornaviruses are candidate helper viruses for scKoV. In conclusion, our study on scKoV provides novel insights into the evolution and diversity of KoVs.

Keywords

49 kolmioviridae, deltavirus, ambisense, bird metagenome

50 **1. Introduction**

51 The family *Kolmioviridae* (KoVs), recently established in the realm *Ribozyviria*, consists of
52 RNA viruses with negative-stranded circular genomes of approximately 1.5-1.7 kb (1). A
53 representative KoV is human hepatitis D virus (HDV), which was first reported in 1977 (2).
54 After the discovery of HDV, no other related viruses were detected for approximately 40 years.
55 However, since 2018, many viruses related to HDV have been discovered in various vertebrates
56 and invertebrates, and currently, KoVs spanning 11 genera, along with additional unassigned
57 viruses, have been identified (1,3–8).

58 KoVs share unique features markedly different from other typical RNA viruses (RNA
59 viruses in the kingdom *Orthornavirae* of the realm *Riboviria*) in terms of their genomes,
60 replication, and transmission. The KoV genome is viroid-like, circular, and single-stranded
61 RNA that exhibits high self-complementarity, forming a rod-like structure (3–9). Unlike other
62 RNA viruses, KoVs only encode the delta antigen (DAg), a nucleocapsid-like protein, and lacks
63 RNA-dependent RNA polymerase, a hallmark of RNA viruses. Consequently, KoVs replicate in
64 the cell nucleus depending on the host DNA-dependent RNA polymerase (DdRp). This unique
65 replication occurs though a rolling-circle replication, utilizing the autocatalytic reaction of
66 ribozymes present in the KoV genome and antigenome. (10,11). As KoVs encode only DAg,
67 and lack proteins required for the formation of virus particles, they rely on the envelope proteins
68 of co-infecting "helper" viruses to produce infectious virions. Thus, KoVs are classified as
69 "satellite" viruses (5,12,13).

70 KoVs may utilize unique coding strategies to provide proteins essential for replication,
71 given the constraints of their small, highly self-complementary genomes. HDV expresses two
72 isoforms of the DAg, known as small and large DAg (S-HDAg and L-HDAg), through A-to-I
73 RNA editing, which is mediated by the host enzyme ADAR1 and modified the stop codon of S-

74 HDAg ORF (14–17). As a result, L-HDAg contains a 19-amino-acid extension at its C-terminus
75 that includes a nuclear export signal (18) and a farnesylation site which is required to interact
76 with helper virus envelope proteins (19). HDV utilizes these two isoforms to finely regulate
77 genome replication and virion formation. Although this RNA editing mechanism has only been
78 observed in HDV, other KoVs might employ different strategies to expand their coding capacity.
79 For example, Swiss snake colony virus 1 was reported to express two isoforms of DAg,
80 although the underlaying mechanisms remain unclear (20). Further, several KoVs, such as
81 DrDV-B, possess additional relatively long ORFs in their genomes (5,21). However, these
82 ORFs have yet to be shown to be expressed as mRNA, and there is no evidence that they are
83 functional viral genes.

84 The Serinus canaria-associated deltavirus (following the establishment of the family
85 *Kolmioviridae*, we designates it as Serinus canaria-associated kolmiovirus [scKoV]) was recently
86 identified through large-scale analysis of publicly available RNA-seq data, but its characteristics
87 are largely unclear (3). In the previous study, only partial sequences corresponding to the
88 transcript encoding DAg were identified. However, the rapid increase in publicly available
89 RNA-seq data offers an opportunity to identify the complete viral genome and conduct more
90 detailed analyses (22). Further, scKoV was suspected to have originated from contaminants in
91 the previous study, as it was only detected in a single RNA-seq dataset from canary skin and is
92 genetically distinct from viruses of the genus *Perithurisazvirus*, authentic avian KoVs (3) (Fig.
93 1). Thus, reanalyzing scKoV with the ever-increasing RNA-seq data may help clarify its origin.

94 In this study, we analyzed public RNA-seq data and identified multiple complete genome
95 sequences of scKoV. We provided strong evidence that scKoV is an authentic avian virus.
96 Further, we showed that scKoV transcribes a genomic-sense mRNA that encodes a novel gene
97 (ORF2) in addition to the well-known antigenomic-sense mRNA encoding DAg. We also

98 revealed that the ORF2 gene appears to express two protein isoforms via alternative splicing.
99 Our findings highlight an adaptive strategy by which KoVs maximize their gene-coding
100 capacity under the constraints of their small and highly self-complementary genomes.
101

102 ## 2. Results

103 ### *2.1. scKoV-derived reads were identified in multiple bird public RNA-seq datasets.*

104 As described above, the previous study detected scKoV in only one RNA-seq dataset. To further
105 identify scKoV-positive RNA-seq datasets, we mapped 15,452 publicly available bird RNA-seq
106 datasets to the partial sequence of scKoV (BR001664.1). A total of 66 RNA-seq datasets were
107 found to contain scKoV-derived reads, including the dataset in which scKoV was initially
108 identified in the previous study (Tables 1 and S1).

109 The scKoV-reads were found in four bird species: the common canary (*Serinus canaria*
110 [Linnaeus, 1758]), European serin (*Serinus serinus* [Linnaeus, 1766]), and house finch
111 (*Haemorhous mexicanus* [Statius Müller, 1776]) in the order *Passeriformes* and monk parakeet
112 (*Myiopsitta monachus* [Boddaert, 1783]) in the order *Psittaciformes*. The scKoV-positive RNA-
113 seq datasets were distributed across five BioProjects deposited by four independent research
114 groups (PRJNA300534 and PRJNA591356 were deposited by the same group), suggesting that
115 the scKoV-positive birds originated from diverse sources.

116 The scKoV-positive RNA-seq datasets were derived not only from skin samples but also in
117 various tissues including fat tissue, blood, brain, lung, and ovary. This strongly suggests that
118 scKoV is not a result of body-surface contamination but likely infects birds, potentially causing
119 systemic infection and/or viremia. These findings indicate that scKoV circulates among a broad
120 range of avian hosts, spanning different taxonomic orders.
121

122 ***2.2. The complete genome sequences of scKoV were identified.***

123 To obtain complete genome sequences of scKoV, each scKoV-positive RNA-seq dataset was
124 assembled. Among the resultant contigs, six contigs were identified as potential complete scKoV
125 genome sequences. Self-dotplot analyses revealed identical sequences at both ends of each contig
126 (Fig. S1), suggesting that they are circular contigs. We mapped the original RNA-seq datasets
127 back to the circularized contigs, confirming that multiple reads spanned the junctions
128 appropriately. These data strongly suggest that the contigs are indeed circular genomes.

129 To obtain additional complete scKoV genomes, we mapped scKoV-positive RNA-seq
130 datasets, from which no complete scKoV genomes had been obtained above, to the circularized
131 complete genomes of scKoV and extracted the consensus sequences. As a result, a total of 16
132 complete scKoV genomes were reconstructed from the RNA-seq datasets of *S. canaria*, *H.*
133 *mexicanus*, and *M. monachus* (Table 1). Notably, by this mapping-based method, we succesfully
134 recovered the complete scKoV genome from the RNA-seq datasets where only the partial
135 sequence had been initially reported in the previous study (3).

136

137 ***2.3. Genetically diverse scKoV circulate among multiple bird species.***

138 To elucidate the evolutionary relationships among scKoVs, we performed a phylogenetic analysis
139 using the complete nucleotide sequences of scKoV genomes. The resulting phylogenetic tree
140 showed three distinct clusters of scKoVs, designated as genotype 1, 2, and 3 (Fig. 2A). The
141 genotype 1 included scKoVs identified in all the three bird species (*S. canaria*, *H. mexicanus*, and
142 *M. monachus*), while the genotypes 2 and 3 were exclusively found in scKoVs from *S. canaria*
143 and *M. monachus*, respectively. Pairwise nucleotide sequence comparisons revealed high
144 nucleotide sequence identities (>95%) within each genotype, whereas inter-genotype nucleotide

145 sequence identities were <84% between genotypes 1 and 2, <83% between genotypes 1 and 3,
146 and <89% between genotypes 2 and 3 (Fig. 2B).

147 We also obtained data indicating that multiple genotypes of scKoV existed within individual
148 hosts. For example, all scKoV-positive RNA-seq datasets from BioProject PRJNA679636
149 originated from a single individual (23) , and both genotypes 1 and 3 were detected within these
150 datasets (Table 1). We thus investigated whether multiple genotypes of scKoV coexisted within
151 each scKoV-positive sample. The scKoV-positive RNA-seq datasets from BioProjects
152 PRJNA591356, PRJNA939570, and PRJNA679636 were mapped to the genomes of distinct
153 genotypes detected within the same BioProjects in a manner that ensures unique alignment to the
154 best match. The results indicated the coexistence of two genotypes of viruses within individual
155 RNA-seq data in varying ratios, with some data showing nearly a 1:1 ratio of mixed genotypes
156 (Fig. 2C). Apparently, these RNA-seq data were not derived from pooled samples of multiple
157 individuals based on the available metadata and literatures. Taken together, these findings suggest
158 that multiple genotypes of scKoV circulate among the birds and may occasionally cause mixed
159 infections.

160

161 ***2.4. scKoV potentially infects to various tissues.***

162 To understand the tissue tropism of scKoV, we analyzed the number of scKoV-derived reads
163 across the scKoV-positive RNA-seq datasets from BioProject PRJNA679636, which were
164 derived from various tissues of a single individual (23). The reads per million (RPM) of scKoV
165 was highest in the brain (264.1 RPM in the forebrain and 121.9 RPM in the cerebellum), followed
166 by the lung (164.1 RPM) and ovary (77.3 RPM), while only a small number of scKoV reads were
167 detected in the liver (0.2 RPM) and muscle (5.5 RPM) (Tables 1 and S1 and Fig. 2C). Moderate

168 amounts of scKoV reads were detected in the kidney (25.2 RPM), heart (22.7 RPM), and spleen
169 (21.8 RPM). These results suggest that scKoV infects a broad range of tissues.
170
171 ***2.5. scKoV exhibits ambisense gene coding and utilizes alternative splicing.***
172 We next characterized the genome structures of scKoV, revealing that the typical characteristics
173 of KoVs are conserved in scKoVs as follows. The scKoV genomes were approximately 1,670 bp
174 in length, with a GC content of approximately 55%, consistent with other KoV members (3–8).
175 The high self-complementarity of the circular genome, a typical feature of KoVs, was also
176 conserved in scKoV (Figs. 3A and S2). The relative positions of the DAg-encoding ORF, the
177 downstream poly-A signal, and both the genomic and antigenomic ribozymes were consistent
178 with those of other typical KoVs (Fig. 3B). Additionally, the predicted scKoV ribozymes exhibit
179 the conserved HDV ribozyme class, unlike toad and termite KoVs, which retain type III
180 hammerhead ribozymes (24) (Figs. 3C and S3). The ribozymes of scKoV contain sequence
181 variations, but these are expected to have minimal effects on their secondary structures (Fig. S3).
182 Notably, two additional ORFs (tentatively named ORF2 and ORF3) were identified on both
183 the genomic- and antigenomic-senses, respectively, which were located in the self-
184 complementary region of the DAg ORF (Figs. 3A and 3B). ORF2 is conserved in all scKoVs,
185 whereas ORF3 is absent in one virus (BR002468.1, assembled from SRR13480248) (Fig. S4).
186 Moreover, an additional poly-A signal was located immediately downstream of ORF2 (Fig. 3B).
187 To elucidate the transcriptional patterns of scKoVs, we mapped scKoV-positive RNA-seq
188 datasets to the corresponding viral genomes. The results exhibited a bimodal mapping pattern
189 (Fig. S5), suggesting the presence of a novel transcript in addition to the one encoding DAg. To
190 further characterize the putative novel transcript, we mapped strand-specific RNA-seq datasets
191 (BioProjects PRJNA591356 and PRJNA939570) to the corresponding viral genomes. The

192 mapping patterns clearly indicated the presence of a genomic-sense transcript encoding ORF2, as
193 well as the typical antigenomic-sense transcript encoding DAg (Figs. 3D and S5). The boundary
194 between the genomic and antigenomic transcripts was estimated to be located at the edge of the
195 rod-like structure of the scKoV genome, which is thought to function as a transcriptional promoter
196 (25). The edge of the rod in scKoV largely retained the conserved domains previously reported
197 in HDVs (Fig. S6) (25). Furthermore, based on the mapping patterns of the RNA-seq data in
198 BioProject PRJNA591356, the transcription start sites of the genomic- and antigenomic-sense
199 transcripts were predicted to be located between the internal and external bulges of the rod edge
200 (Fig. 3E). These data strongly suggest that scKoV expresses a genomic-sense transcript encoding
201 ORF2.

202 The mapping results also showed several putative splicing junctions. Among them, the one
203 located in the genomic-sense ORF2 transcript is prominent and reliable, as a large number of
204 reads consistently spanned the junction across all the RNA-seq data (Figs. 3D and S5). The
205 putative intron retains the typical features of major eukaryotic introns, including the GU-AG
206 motifs of donor/acceptor sites and a polypyrimidine tract present upstream of the AG motif at the
207 end of the intron (Fig. 3F) (26). Notably, the spliced ORF2 transcript encodes a protein that differs
208 from the unspliced ORF2 transcript in its C-terminal region (Fig. 3D and Table S2).

209 To investigate the function of the putative proteins translated from unspliced and spliced
210 ORF2 transcripts (designated ORF2a and ORF2b, respectively), we first performed sequence
211 similarity searches. However, neither protein showed sequence similarity to any known protein.
212 Additionally, no significant biases in hydrophobicity or polarity were observed (Figs. S7A and
213 S7B). We also carried out a series of in *silico* analyses, including functional domain searches,
214 predictions of topological structures, nuclear localization signals, and transmembrane domains
215 (Fig. S7C), but could not find any functional domains. An intrinsically disordered region was

216 identified exclusively in the C-terminal third of the ORF2b (Fig. S7D). Additionally, structural
217 predictions indicated that the N-terminus of the ORF2 protein forms a well-defined helical
218 structure, whereas the C-terminus of the ORF2 lacks a defined structure (Fig. S7E). These
219 findings suggest that scKoV expresses genomic-sense transcripts encoding proteins of unknown
220 function.
221
222 ***2.6. No evidence for RNA-editing was found on the stop codon of DAg.***
223 HDV utilizes the host A-to-I RNA editing machinery at the stop codon of DAg to express the
224 larger isoform of DAg protein. To investigate whether scKoV also employs A-to-I RNA editing,
225 we analyzed nucleotide variations at the stop codons of each ORF using the mapping data. Base
226 variations (A-to-G or T-to-C), potentially resulting from A-to-I editing of the genome or antigenome,
227 were observed in 11 out of the 16 mapping datasets (Table S3). However, except for SRR23747114,
228 the stop codons of the extended DAg ORFs, generated by the cancellation of the original stop
229 codon through A-to-I RNA editing, were located downstream of the poly-A signal (Fig. S8). These
230 results suggest that scKoV is unlikely to utilize host A-to-I RNA editing to produce DAg proteins
231 of different lengths.
232
233 ***2.7. Avian bornaviruses are the candidate helper virus for scKoV.***
234 To gain insights into potential helper viruses for scKoV, we searched for co-existing viruses in
235 the scKoV-positive RNA-seq datasets. BLAST searches using the assembled contigs revealed that
236 contigs derived from avian bornaviruses (ABVs), canary bornavirus 1 and 3 (CnBV-1 and -3) and
237 parrot bornavirus 2 (PaBV-2) (the genus *Orthobornavirus* of the family *Bornaviridae*) were
238 detected in 64 out of 66 scKoV-positive datasets (Figs. 4A and S9). CnBV-1 and 3 were detected
239 in the RNA-seq datasets from *S. canaria*, *S. serinus*, and *H. mexicanus* (the order *Passeriformes*),

240 while PaBV-2 was detected in the data from *M. monachus* (the order *Psittaciformes*). No other
241 enveloped viruses were identified. We also analyzed the correlation between their read counts. As
242 a result, the RPMs of scKoV and ABVs showed a weak positive correlation (Fig. 4B). These
243 results suggest that scKoV may utilize co-infecting ABVs as helper viruses.
244

245 **3. Discussion**

246 Although many novel KoVs have been identified recently, the diversity of KoVs remains unclear
247 since some KoVs have not yet been characterized well. We previously identified scKoV from a
248 single canary RNA-seq datasets, which is distantly related to the other avian KoVs, but only a
249 partial sequence corresponding to the DAg mRNA had been identified. In this study, we identified
250 the complete genome sequences of scKoV and revealed its unique genetic features among KoVs.
251 Notably, we showed a series of evidence strongly suggesting that scKoV expresses genomic-sense
252 transcripts encoding proteins of unknown function, designated ORF2, besides the antigenomic-
253 sense transcript encoding DAg (Figs. 3B and 3D). Although KoVs are currently classified as
254 negative-strand RNA viruses, our findings strongly suggest that scKoV is an ambisense virus.
255 Furthermore, our data indicate that the genomic-sense transcript undergoes alternative splicing,
256 potentially encoding two ORF2 protein isoforms. Therefore, scKoV employs a unique strategy to
257 maximize its coding capacity under the constraints of its small and self-complementary circular
258 genome.

259 Some other KoVs might adopt a similar coding strategy. For instance, some KoVs, including
260 bat deltavirus B, Chinese fire belly newt virus 1, and ray-finned fish virus 1, have been reported
261 to possess genomic-sense ORFs at positions similar to those of the scKoV ORF2 and poly-A
262 signals (Fig. S10) (6,8). However, their mapping patterns did not show a clear bimodal
263 distribution (Fig. S10), suggesting that these ORFs may not be transcribed. Because these RNA-

264 seq libraries were generated via rRNA depletion rather than poly-A enrichment, we cannot
265 exclude the possibility that the data do not reflect actual transcription. Moreover, in DrDV-B, the
266 start codon of ORF2 is not conserved across all viral strains (Fig. S11A). Additionally, these
267 genomic-sense ORFs showed no similarity in either secondary or 3D structure to scKoV ORF2
268 (Figs. S11B and S11C), suggesting that these viruses may lack conserved genes. Further studies
269 are required to assess the above possibility, which would contribute to a deeper understanding of
270 the diverse replication strategies of KoVs.

271 Our results strongly suggest that the promoter of scKoV could initiate bidirectional
272 transcription. HDV transcribes mRNA using the host DdRp, with the rod-like edge of its circular
273 RNA genome functioning as a transcriptional promoter, and the promoter on the genomic-strand
274 initiate the transcription of antigenomic-strand mRNA (25). In scKoV, the mapping pattern clearly
275 revealed that the transcripts were expressed in both the genomic- and antigenomic-senses, with
276 the edge of the rod-like structure serving as the boundary (Figs. 3D and 3E). Some RNA-seq
277 datasets showed that the approximate initiation sites of both the genomic- and antigenomic-sense
278 transcripts are located between the internal and external bulges at edge of the rod-like structure,
279 which is close to the location previously identified in HDV (25). Although further experiments
280 are necessary, these observations suggest that both the genomic and antigenomic rod edges of
281 scKoV possess distinct promoter activity. The presence of KoVs with bidirectional and
282 monodirectional promoters provides valuable insights into their evolutionary processes and
283 difference in replication strategies.

284 Our mapping analyses revealed potential splicing events in the genomic transcripts of scKoV.
285 While the majority of RNA viruses replicate in the host cytoplasm, a few lineages, such as KoVs,
286 bornaviruses, orthomyxoviruses, and some rhabdoviruses, transcribe in the host cell nucleus and
287 employ the host splicing machinery, which occurs inside of the nucleus, to express multiple

288 proteins from the same genomic regions (27–30). However, evidence for alternative splicing in
289 KoVs has been lacking thus far. Here, we identified a putative splicing site in the scKoV ORF2
290 gene (Figs. 3D and 3F), which may lead to the expression of two isoforms of ORF2 proteins (Fig.
291 3D). Thus, this study provides the first evidence that KoV utilizes alternative splicing and
292 emphasizes the need for future characterization of other KoV strains, considering the potential
293 use of alternative splicing mechanisms.

294 The ambisense coding strategy of scKoV is analogous to that of other circular RNA viruses.
295 KoVs share the genome structure and the replication mechanism with circular RNA replicons,
296 including viroids, virusoids, and other unclassified mobile genetic elements (31,32). Recent
297 studies have revealed an unprecedented diversity of circular RNA replicons (33–35). Among the
298 newly identified circular RNA viruses, fungal viruses in the phylum *Ambiviricota* (the kingdom
299 *Orthornavirae* of the realm *Riboviria*) possess at least two non-overlapping ambisense ORFs, one
300 of which encodes a distinct viral RdRp, suggesting their role as evolutionary intermediates (34,36).
301 The genome of scKoV exhibits a similar organization to that of ambiviruses, with the two ORFs
302 (DAg and ORF2) arranged in an ambisense orientation within a self-complementary region (Fig.
303 3). This suggests that ambisense coding strategies may be common among certain circular RNA
304 viruses.

305 Our findings strongly suggest that birds are the authentic host of scKoV. The previous study
306 proposed the possibility that scKoV does not infect canaries but rather originates from
307 contaminants, based on the following two points: (i) scKoV is distantly related to tgDeV, which
308 is an authentic avian virus found in a wide range of passerine birds; (ii) scKoV was detected only
309 in a single RNA-seq dataset obtained from canary skin (3). However, our study identified scKoV
310 in several passerine birds, including canaries, as well as in a parrot (Tables 1 and S1). Additionally,
311 scKoV was detected not only in the skin but also in multiple parenchymal organs, fat tissue, and

312 blood (Tables 1 and S1). Furthermore, the bimodal transcription patterns observed for scKoV
313 suggest active transcription of viral mRNA in those tissues (Fig. 3D). These findings strongly
314 suggest that scKoV is an authentic avian virus rather than a contaminant. The existence of avian
315 kolmioviruses that are phylogenetically distinct from the lineages of known reptilian, avian, and
316 mammalian KoVs (Fig. 1), suggests that KoVs infecting the above-mentioned animals are far
317 more genetically diverse than previously thought. Further studies on KoVs are required to
318 understand their host range and genetic diversity.

319 The identification of the complete scKoV genome will contribute to updating the taxonomy
320 of KoVs. The current genus demarcation criterion established by the International Committee on
321 Taxonomy of Viruses (ICTV) is DAg with ≤60% amino acid sequence identity (1). Thus, scKoV
322 is classified as a new genus because its DAg sequence identity to other KoVs is below 40% (3).
323 We further demonstrated the presence of genetic diversity within scKoVs. The ICTV species
324 demarcation criteria require ≤80% nucleotide genome identity and ≤70% S-DAg amino acid
325 identity (1). Based on these criteria, the three groups of scKoV are classified as different
326 genotypes of the same species (Fig. 2B). Given the limited information on viral genome sequences
327 for classifying KoVs into distinct species within the same genus, our findings on scKoV sequence
328 diversity may help refine future classification criteria for KoVs.

329 Our study revealed that scKoV has a broad host range and the potential for interspecies
330 transmission. Our findings suggest that scKoV, particularly genotype 1, is capable of interspecies
331 transmission between birds of different orders (Fig. 2A). It has been suggested that KoVs have
332 evolved through the multiple interspecies transmission (3,8). Thus, evidence of relatively recent
333 inter-order transmission of scKoV may provide insights into the evolutionary history of KoVs.
334 Further detailed analyses of the host specificity of scKoV are necessary.

335 We also reveal the mixed infections of different genotypes of scKoV in some individuals.
336 scKoVs of different genotypes were detected mixed within RNA-seq data from the same
337 individual (Fig. 2C). These mixed infections, observed across multiple BioProjects and in some
338 cases with nearly equal ratios and certain read numbers of different genotypes, suggest that they
339 are unlikely to be due to contamination and/or index hopping during sampling, library preparation,
340 and sequencing processes. HDV has been reported to undergo recombination between different
341 genotypes during coinfection (37). Our findings of mixed infection with scKoVs belonging to
342 different genotypes provide important insights into the epidemiology and evolution of KoVs.

343 Our study identified ABVs as candidate helper viruses for scKoV. The helper viruses for
344 non-HDV KoVs remain largely unknown except for snake deltavirus that utilizes the envelope
345 proteins of co-infected reptarenavirus or hartmanivirus in the family *Arenaviridae* (5,13). Our
346 previous study indicated co-existence of scKoV with CnBV in a single RNA-seq dataset
347 (SRR2915371); however, this RNA-seq dataset was derived from a pooled sample from multiple
348 individuals, and no definitive evidence of co-infection between scKoV and CnBV was obtained
349 (3). In this study, we identified CnBV-1, CnBV-3 and PaBV-2, which encode envelope
350 glycoproteins, in 64 out of 66 scKoV-positive RNA-seq datasets (Figs. 4A and S8). Notably,
351 except for the RNA-seq dataset in which scKoV was previously identified (3), none of these were
352 clearly from pooled samples. Although further experimental validation is needed, these results
353 suggest that ABVs are helper viruses for scKoV. Further, our data provide insights into the
354 hypothesis that KoVs have evolved with diverse satellite-helper relationships.

355 Co-infection with scKoV and ABV suggests that the pathogenicity of scKoV in infected
356 birds needs to be considered. Co-infection of HDV and HBV accelerates the pathogenic effects
357 of HBV, leading to severe or fulminant hepatitis and progression to hepatocellular carcinoma (38).
358 The pathogenicity of scKoV remains unknown due to the lack of metadata clarifying whether

359 scKoV-positive RNA-seq data were obtained from healthy birds. In contrast, the co-infecting
360 PaBV is a causative agent of proventricular dilatation disease (PDD), an immune-mediated
361 inflammatory disease (39,40). Similarly, CnBV was also reported to be associated with PDD in
362 canaries, but experimental infections using a CnBV isolate have not successfully reproduced the
363 pathology, suggesting that other factors may be involved in the onset of the disease (41).
364 Analogous to co-infection of HDV and HBV, scKoV may also contribute to or exacerbate PDD
365 through co-infection with CnBV. Further epidemiological studies of scKoV and CnBV is required
366 to clarify the etiology of PDD.

367 Our analysis suggests that scKoV may have the potential to infect various tissues. While
368 HDV is known for its high tropism for the liver (12), non-HDV KoVs have been detected in
369 multiple organs (3,7,8,13). Like other non-HDV KoVs, scKoV was found to predominantly target
370 the skin, fat tissue, blood, and some parenchymal organs, rather than the liver (Table 1 and Fig.
371 2C). ABVs, candidate helper viruses for scKoV, can also infect various organs (41,42). Our results
372 support the hypothesis that while the tissue tropism of scKoV and other KoVs is broad, it is likely
373 dependent on the tissue infectivity of the helper virus (3,7,13).

374 Taken together, we provide novel insights into the genomic features, replication strategies,
375 epidemiology, and satellite-helper relationships of KoVs through the comprehensive and detailed
376 analyses of the complete scKoV genomes. Further analyses are needed to explore the broader
377 diversity of KoVs.

378

379 **4. Materials and Methods**

380 ***4.1. Detection of scKoV-derived reads from public RNA-seq data***

381 RNA-seq data from birds (in the class *Aves* without *Gallus gallus* [Linnaeus, 1758]) were
382 downloaded from the NCBI Sequence Read Archive (43) (accessed on Jan 20, 2024) and mapped

383 to the partial scKoV genome (BR001664.1) using Magic-BLAST v1.7.1 (44) with the options "-
384 splice T -word_size 16 -lcase_masking". The mapped read numbers were counted using
385 SAMtools v1.19 (45). The mapping results were manually verified, and reads that were locally
386 aligned to sequences of less than 25 bases in the reference were excluded as non-specific mapping.
387

388 ***4.2. Identification of complete scKoV genomes***

389 The scKoV-positive RNA-seq data were downloaded and dumped using SRA Toolkit
390 (https://github.com/ncbi/sra-tools), which were preprocessed using fastp v0.23.4 (46) with the
391 options "-l 35 -x -y". The preprocessed reads were mapped to the host genome sequences using
392 HISAT2 v2.2.1 (47) with the default settings. The unmapped reads were extracted with SAMtools
393 v1.19 and subjected to *de novo* assembly using Trinity v2.15.1 (48) with the default settings. The
394 scKoV contigs were identified through a two-step sequence similarity search: BLASTn against
395 the partial scKoV genome and BLASTx against the clustered nr database (43), using BLAST+
396 v2.15.0 (49).

397 Self-dotplot analysis of the linear scKoV contigs was performed using the YASS program
398 with the default settings (50). Contigs with identical ends were manually circularized using
399 Geneious Prime v2024.0.5 (https://www.geneious.com). The circularities of scKoV contigs were
400 further verified by mapping short reads to the circularized scKoV contigs using Geneious and
401 manually checking the mapped reads across the circularized boundaries.

402 For RNA-seq data where circularized scKoV contigs could not be obtained by *de novo*
403 assembly, the scKoV-positive RNA-seq data were mapped to the circular scKoV contigs using
404 Geneious and extracted the circular consensus sequences.

405 For all the contigs, all positions were confirmed to be covered with at least three reads.
406

407 ***4.3. Phylogenetic analysis***

408 Phylogenetic relationship among all known KoVs were inferred as follows. The amino acid
409 sequences of KoV DAg were aligned by MAFFT v7.490 with the E-INS-I algorithm (51). The
410 phylogenetic tree was constructed using the Bayesian Markov chain Monte Carlo (MCMC)
411 method in MrBayes version 3.2.7a (52) with two independent runs, four chains per run, and the
412 JTT model of substitution. The analysis was run for 5 million iterations, with samples taken every
413 5,000 steps. The average standard deviation of split frequencies was 0.010.

414 For the nucleotide sequences of the full-length scKoV genomes, multiple sequence
415 alignment was performed using MAFFT v7.490 with the E-INS-I algorithm (51). Pairwise
416 sequence identities were calculated based on the alignment using Geneious. A maximum-
417 likelihood tree was constructed using the TVM+I+G4 model, selected as the best-fit model based
418 on the minimum AIC in RAxML v1.1.0 (53). The reliability of the tree was assessed by 1,000
419 bootstrap resampling with the transfer bootstrap expectation method (54). Both trees were
420 visualized and annotated in the Interactive Tree Of Life (iTOL) v6.9.1 (55).

421

422 ***4.4. Sequence Characterization***

423 The self-complementarities of scKoV genomes were analyzed using the Mfold web server (56)
424 with the default settings. Genomic and antigenomic ribozyme structures were initially inferred
425 using the IPknot web server (57), with the visualized output from IPknot serving as a guide for
426 manual ribozyme structure drawing. Poly-A signals (AAUAAA) were manually identified in both
427 strands of KoV genomes. ORFs were detected using the 'Find ORF' function in Geneious, with
428 a minimal threshold of 300 nucleotides. ORFs that overlap with the terminal rod-like structure of
429 the viral genome, where the putative transcriptional promoter is located, poly(A) signal, or the
430 predicted ribozyme regions were excluded.

431

432 ***4.5. Short read mapping to analyze mixed infection with scKoV of different genogroups.***

433 The short reads from scKoV-positive RNA-seq data belonging to BioProjects PRJNA591356,
434 PRJNA939570, and PRJNA679636 were mapped to scKoV sequences of different genogroups
435 detected from the same BioProject (scKoV from SRR10526804 and SRR10526851 for
436 PRJNA591356, scKoV from SRR23747122 and SRR23747110 for PRJNA939570, scKoV from
437 SRR13480248 and SRR13480240 for PRJNA679636). Mapping was performed using of HISAT
438 ver 2.2.1. with the `-k 1` option. The mapped read numbers were counted using SAMtools v1.19
439 (45). The data with RPM>10 were visualized.

440

441 ***4.6. Short read mapping to analyze transcriptional patterns***

442 The short reads from scKoV-positive RNA-seq data were preprocessed as described above (see
443 the section 4.2) and mapped to the corresponding scKoV genomes using HISAT2 v2.2.1 (47) with
444 the options "-k 2 --max-intronlen 1000 --rna-strandness RF". To accurately evaluate reads
445 spanning the circularized genome boundaries, 2x tandemly repeated genomes were used as the
446 references. The "-k 2" option in HISAT2 was selected to ensure precise mapping to the 2x
447 genomes. For strand-specific RNA-seq data, the "--rna-strandness RF" option was also used to
448 retain strand information. The mapped reads were counted using SAMtools v1.19 (45).

449

450 ***4.7. Characterization of ORF2 proteins***

451 The amino acid sequences of both ORF2a and ORF2b were analyzed using BLASTp, employing
452 the PSI-BLAST and the DELTA-BLAST algorithms with an e-value threshold of < 0.05.
453 Theoretical molecular weight and isoelectric point was calculated using ProtParam web server
454 (https://web.expasy.org/protparam/). Amino acid sequence alignments, colored according to

455 hydrophobicity and polarity, were generated using Geneious. Membrane topology of ORF2 proteins
456 was inferred using DeepTMHMM ver. 1.0 (58). Nuclear localization signal was inferred using the
457 cNLS mapper web server with a cut-off value of 3.0 (59). Intrinsically disordered region were
458 predicted using AIUPred web server (60). Secondary structures of ORF2 proteins were predicted using
459 JPred v4 (61).Protein structure predictions were performed by AlphaFold3 web server (62).
460

461 ***4.8. Detection of RNA-editing on the stop codon of DAg***

462 Sequence variations at the DAg stop codon were identified in the mapping data of section 4.5
463 using 'Find SNP/Variants' in Geneious.
464

465 ***4.9. Detection of co-existing viruses***

466 To identify co-existing viruses in scKoV-positive RNA-seq data, the assembled contigs (see the
467 section 4.2) were clustered using CD-HIT v 4.8.1 (63) with the 95 % threshold. The clustered
468 contigs of 500 nucleotides or longer were extracted using SeqKit v2.4.0 (64), which were
469 subjected to a two-step sequence similarity search. The first search was conducted by MMseqs2
470 (version c48da9d781b81804727b5cccfed7f97cfcc20c9d) (65) with the default settings against a
471 custom database consisting of viral protein sequences with a threshold E-value of 0.001. The
472 custom database was created as follows. Viral protein sequences were downloaded from the NCBI
473 nr database on June 22, 2023, which was clustered by using CD-HIT v4.8.1 (63) with a threshold
474 of 0.9. Contigs alignable to viral sequences other than retroviruses and environmental viruses
475 were extracted. The second BLASTx search was then performed using the extracted contigs as
476 queries against the NCBI clustered nr database (43) with the options "-e-value < 1e-4 -word_size
477 2 -max_target_seqs 10" on Aug 26, 2024. The contigs with the best hit to viruses were extracted
478 and manually analyzed. Contigs with the best hit to bornaviruses (the family *Bornaviridae*) were

479 further subjected to a BLASTn search against a database of CnBVs and PaBVs to accurately
480 identify the species/genotypes.
481 To quantify ABVs-derived reads in scKoV-positive RNA-seq data, preprocessed reads were
482 mapped using HISAT2 (47) with the option "-k 1" against CnBV-1 (NC_030690.1), CnBV-3
483 (NC_024296.1), and newly obtained PaBV contig assembled from SRR13480248
484 (Supplementary Materials) because the genome sequence of co-existed PaBV is slightly different
485 from the ones deposited in INSDC.
486
487
488 **Acknowledgements**
489 The super-computing resources were provided by Human Genome Center, the Institute of
490 Medical Science, the University of Tokyo.
491 This study was supported by KAKENHI grant numbers 21H01199 (MH), 22K19234 (MI
492 and MH), 23K20902 (MH), 24K21922 (MH), and 24K18455 (MK) and the 2024 Osaka
493 Metropolitan University (OMU) Strategic Research Promotion Project (Young Researcher) (MK).
494

495 **References**

496 1. Kuhn JH, Babaian A, Bergner LM, Dény P, Glebe D, Horie M, et al. ICTV Virus
497 Taxonomy Profile: Kolmioviridae 2024. J Gen Virol. 2024;105(2):001963.
498 2. Rizzetto M, Canese MG, Aricò S, Crivelli O, Trepo C, Bonino F, et al.
499 Immunofluorescence detection of new antigen-antibody system (delta/anti-delta)
500 associated to hepatitis B virus in liver and in serum of HBsAg carriers. Gut. 1977
501 Dec 1;18(12):997–1003.
502 3. Iwamoto M, Shibata Y, Kawasaki J, Kojima S, Li YT, Iwami S, et al. Identification
503 of novel avian and mammalian deltaviruses provides new insights into deltavirus
504 evolution. Virus Evol. 2021 Jan 20;7(1):veab003.
505 4. Wille M, Netter HJ, Littlejohn M, Yuen L, Shi M, Eden JS, et al. A Divergent
506 Hepatitis D-Like Agent in Birds. Viruses. 2018 Dec;10(12):720.
507 5. Hetzel U, Szirovicza L, Smura T, Prähauser B, Vapalahti O, Kipar A, et al.
508 Identification of a Novel Deltavirus in Boa Constrictors. mBio. 2019 Apr
509 2;10(2):10.1128/mbio.00014-19.
510 6. Chang WS, Pettersson JHO, Le Lay C, Shi M, Lo N, Wille M, et al. Novel
511 hepatitis D-like agents in vertebrates and invertebrates. Virus Evol. 2019 Jul
512 1;5(2):vez021.
513 7. Paraskevopoulou S, Pirzer F, Goldmann N, Schmid J, Corman VM, Gottula LT, et
514 al. Mammalian deltavirus without hepadnavirus coinfection in the neotropical
515 rodent Proechimys semispinosus. Proc Natl Acad Sci. 2020 Jul 28;117(30):17977–
516 83.

517 8. Bergner LM, Orton RJ, Broos A, Tello C, Becker DJ, Carrera JE, et al.
518 Diversification of mammalian deltaviruses by host shifting. Proc Natl Acad Sci.
519 2021 Jan 19;118(3):e2019907118.
520 9. Wang KS, Choo QL, Weiner AJ, Ou JH, Najarian RC, Thayer RM, et al. Structure,
521 sequence and expression of the hepatitis delta (δ) viral genome. Nature. 1986
522 Oct;323(6088):508–14.
523 10. Macnaughton TB, Beard MR, Chao M, Gowans EJ, Lai MMC. Endogenous
524 Promoters Can Direct the Transcription of Hepatitis Delta Virus RNA from a
525 Recircularized cDNA Template. Virology. 1993 Oct 1;196(2):629–36.
526 11. Jeng KS, Daniel A, Lai MM. A pseudoknot ribozyme structure is active in vivo
527 and required for hepatitis delta virus RNA replication. J Virol. 1996
528 Apr;70(4):2403–10.
529 12. Asselah T, Rizzetto M. Hepatitis D Virus Infection. N Engl J Med. 2023 Jul
530 5;389(1):58–70.
531 13. Szirovicza L, Hetzel U, Kipar A, Martinez-Sobrido L, Vapalahti O, Hepojoki J.
532 Snake Deltavirus Utilizes Envelope Proteins of Different Viruses To Generate
533 Infectious Particles. mBio. 2020 Mar 17;11(2):e03250-19.
534 14. Bergmann KF, Gerin JL. Antigens of Hepatitis Delta Virus in the Liver and Serum
535 of Humans and Animals. J Infect Dis. 1986 Oct 1;154(4):702–6.
536 15. Bonino F, Heermann KH, Rizzetto M, Gerlich WH. Hepatitis delta virus: protein
537 composition of delta antigen and its hepatitis B virus-derived envelope. J Virol.
538 1986 Jun;58(3):945–50.

539 16. Wong SK, Lazinski DW. Replicating hepatitis delta virus RNA is edited in the
540 nucleus by the small form of ADAR1. Proc Natl Acad Sci. 2002 Nov
541 12;99(23):15118–23.
542 17. Taylor JM. Infection by Hepatitis Delta Virus. Viruses. 2020 Jun;12(6):648.
543 18. Lee CH, Chang SC, Wu CHH, Chang MF. A Novel Chromosome Region
544 Maintenance 1-independent Nuclear Export Signal of the Large Form of Hepatitis
545 Delta Antigen That Is Required for the Viral Assembly *. J Biol Chem. 2001 Mar
546 1;276(11):8142–8.
547 19. O'Malley B, Lazinski DW. Roles of Carboxyl-Terminal and Farnesylated Residues
548 in the Functions of the Large Hepatitis Delta Antigen. J Virol. 2005 Jan
549 15;79(2):1142–53.
550 20. Khalfi P, Denis Z, McKellar J, Merolla G, Chavey C, Ursic-Bedoya J, et al.
551 Comparative analysis of human, rodent and snake deltavirus replication. PLOS
552 Pathog. 2024 Mar 5;20(3):e1012060.
553 21. Khalfi P, Denis Z, Merolla G, Chavey C, Ursic-Bedoya J, Soppa L, et al.
554 Unraveling human, rodent and snake Kolmioviridae replication to anticipate cross-
555 species transmission [Internet]. bioRxiv; 2023 [cited 2023 Oct 20]. p.
556 2023.05.17.541162. Available from:
557 https://www.biorxiv.org/content/10.1101/2023.05.17.541162v1
558 22. Kawasaki J, Kojima S, Tomonaga K, Horie M. Hidden Viral Sequences in Public
559 Sequencing Data and Warning for Future Emerging Diseases. mBio. 2021 Aug
560 17;12(4):10.1128/mbio.01638-21.

561 23. Huang Z, De O. Furo I, Liu J, Peona V, Gomes AJB, Cen W, et al. Recurrent
562 chromosome reshuffling and the evolution of neo-sex chromosomes in parrots. Nat
563 Commun. 2022 Feb 17;13(1):944.
564 24. de la Peña M, Ceprián R, Casey JL, Cervera A. Hepatitis delta virus-like circular
565 RNAs from diverse metazoans encode conserved hammerhead ribozymes. Virus
566 Evol. 2021 Jan 20;7(1):veab016.
567 25. Beard MR, MacNaughton TB, Gowans EJ. Identification and characterization of a
568 hepatitis delta virus RNA transcriptional promoter. J Virol. 1996 Aug;70(8):4986–
569 95.
570 26. Wilkinson ME, Charenton C, Nagai K. RNA Splicing by the Spliceosome. Annu
571 Rev Biochem. 2020 Jun 20;89(Volume 89, 2020):359–88.
572 27. Dubois J, Terrier O, Rosa-Calatrava M. Influenza Viruses and mRNA Splicing:
573 Doing More with Less. mBio. 2014 May 13;5(3):10.1128/mbio.00070-14.
574 28. Schneider PA, Schneemann A, Lipkin WI. RNA splicing in Borna disease virus, a
575 nonsegmented, negative-strand RNA virus. J Virol. 1994 Aug;68(8):5007–12.
576 29. Cubitt B, Oldstone C, Valcarcel J, de la Torre JC. RNA splicing contributes to the
577 generation of mature mRNAs of Borna disease virus, a non-segmented negative
578 strand RNA virus. Virus Res. 1994 Oct 1;34(1):69–79.
579 30. Kuwata R, Isawa H, Hoshino K, Tsuda Y, Yanase T, Sasaki T, et al. RNA Splicing
580 in a New Rhabdovirus from Culex Mosquitoes. J Virol. 2011 Jul;85(13):6185–96.
581 31. Elena SF, Dopazo J, Flores R, Diener TO, Moya A. Phylogeny of viroids,
582 viroidlike satellite RNAs, and the viroidlike domain of hepatitis delta virus RNA.
583 Proc Natl Acad Sci. 1991 Jul;88(13):5631–4.

584 32. Jenkins GM, Woelk CH, Rambaut A, Holmes EC. Testing the Extent of Sequence
585 Similarity Among Viroids, Satellite RNAs, and Hepatitis Delta Virus. J Mol Evol.
586 2000 Jan 1;50(1):98–102.
587 33. Edgar RC, Taylor J, Lin V, Altman T, Barbera P, Meleshko D, et al. Petabase-scale
588 sequence alignment catalyses viral discovery. Nature. 2022 Feb;602(7895):142–7.
589 34. Forgia M, Navarro B, Daghino S, Cervera A, Gisel A, Perotto S, et al. Hybrids of
590 RNA viruses and viroid-like elements replicate in fungi. Nat Commun. 2023 May
591 5;14(1):2591.
592 35. Zheludev IN, Edgar RC, Lopez-Galiano MJ, Peña M de la, Babaian A, Bhatt AS, et
593 al. Viroid-like colonists of human microbiomes [Internet]. bioRxiv; 2024 [cited
594 2024 Aug 29]. p. 2024.01.20.576352. Available from:
595 https://www.biorxiv.org/content/10.1101/2024.01.20.576352v1
596 36. Kuhn JH, Botella L, de la Peña M, Vainio EJ, Krupovic M, Lee BD, et al.
597 Ambiviricota, a novel ribovirian phylum for viruses with viroid-like properties. J
598 Virol. 2024 Jun 10;98(7):e00831-24.
599 37. Wang TC, Chao M. RNA Recombination of Hepatitis Delta Virus in Natural
600 Mixed-Genotype Infection and Transfected Cultured Cells. J Virol. 2005 Feb
601 15;79(4):2221–9.
602 38. Rizzetto M. The adventure of delta. Liver Int. 2016;36(S1):135–40.
603 39. Honkavuori KS, Shivaprasad HL, Williams BL, Quan PL, Hornig M, Street C, et
604 al. Novel Borna Virus in Psittacine Birds with Proventricular Dilatation Disease.
605 Emerg Infect Dis. 2008 Dec;14(12):1883–6.

606 40. Kistler AL, Gancz A, Clubb S, Skewes-Cox P, Fischer K, Sorber K, et al.
607 Recovery of divergent avian bornaviruses from cases of proventricular dilatation
608 disease: Identification of a candidate etiologic agent. Virol J. 2008 Jul 31;5(1):88.
609 41. Rubbenstroth D, Rinder M, Stein M, Höper D, Kaspers B, Brosinski K, et al. Avian
610 bornaviruses are widely distributed in canary birds (*Serinus canaria* f. domestica).
611 Vet Microbiol. 2013 Aug 30;165(3):287–95.
612 42. Gancz AY, Kistler AL, Greninger AL, Farnoushi Y, Mechani S, Perl S, et al.
613 Experimental induction of proventricular dilatation disease in cockatiels
614 (Nymphicus hollandicus) inoculated with brain homogenates containing avian
615 bornavirus 4. Virol J. 2009 Jul 9;6(1):100.
616 43. Sayers EW, Bolton EE, Brister JR, Canese K, Chan J, Comeau DC, et al. Database
617 resources of the National Center for Biotechnology Information in 2023. Nucleic
618 Acids Res. 2023 Jan 6;51(D1):D29–38.
619 44. Boratyn GM, Thierry-Mieg J, Thierry-Mieg D, Busby B, Madden TL. Magic-
620 BLAST, an accurate RNA-seq aligner for long and short reads. BMC
621 Bioinformatics. 2019 Jul 25;20(1):405.
622 45. Danecek P, Bonfield JK, Liddle J, Marshall J, Ohan V, Pollard MO, et al. Twelve
623 years of SAMtools and BCFtools. GigaScience. 2021 Feb 1;10(2):giab008.
624 46. Chen S. Ultrafast one-pass FASTQ data preprocessing, quality control, and
625 deduplication using fastp. iMeta. 2023;2(2):e107.
626 47. Kim D, Paggi JM, Park C, Bennett C, Salzberg SL. Graph-based genome
627 alignment and genotyping with HISAT2 and HISAT-genotype. Nat Biotechnol.
628 2019 Aug;37(8):907–15.

629 48. Grabherr MG, Haas BJ, Yassour M, Levin JZ, Thompson DA, Amit I, et al. Full-
630 length transcriptome assembly from RNA-Seq data without a reference genome.
631 Nat Biotechnol. 2011 Jul;29(7):644–52.
632 49. Camacho C, Coulouris G, Avagyan V, Ma N, Papadopoulos J, Bealer K, et al.
633 BLAST+: architecture and applications. BMC Bioinformatics. 2009 Dec
634 15;10(1):421.
635 50. Noé L, Kucherov G. YASS: enhancing the sensitivity of DNA similarity search.
636 Nucleic Acids Res. 2005 Jul 1;33(suppl_2):W540–3.
637 51. Katoh K, Standley DM. MAFFT Multiple Sequence Alignment Software Version
638 7: Improvements in Performance and Usability. Mol Biol Evol. 2013 Apr
639 1;30(4):772–80.
640 52. Ronquist F, Teslenko M, van der Mark P, Ayres DL, Darling A, Höhna S, et al.
641 MrBayes 3.2: Efficient Bayesian Phylogenetic Inference and Model Choice Across
642 a Large Model Space. Syst Biol. 2012 May 1;61(3):539–42.
643 53. Kozlov AM, Darriba D, Flouri T, Morel B, Stamatakis A. RAxML-NG: a fast,
644 scalable and user-friendly tool for maximum likelihood phylogenetic inference.
645 Bioinformatics. 2019 Nov 1;35(21):4453–5.
646 54. Lemoine F, Domelevo Entfellner JB, Wilkinson E, Correia D, Dávila Felipe M, De
647 Oliveira T, et al. Renewing Felsenstein's phylogenetic bootstrap in the era of big
648 data. Nature. 2018 Apr;556(7702):452–6.
649 55. Letunic I, Bork P. Interactive Tree Of Life (iTOL) v5: an online tool for
650 phylogenetic tree display and annotation. Nucleic Acids Res. 2021 Jul
651 2;49(W1):293–6.

652 56. Zuker M. Mfold web server for nucleic acid folding and hybridization prediction.
653 Nucleic Acids Res. 2003 Jul 1;31(13):3406–15.
654 57. Sato K, Kato Y, Hamada M, Akutsu T, Asai K. IPknot: fast and accurate prediction
655 of RNA secondary structures with pseudoknots using integer programming.
656 Bioinformatics. 2011 Jul 1;27(13):i85–93.
657 58. Hallgren J, Tsirigos KD, Pedersen MD, Armenteros JJA, Marcatili P, Nielsen H, et
658 al. DeepTMHMM predicts alpha and beta transmembrane proteins using deep
659 neural networks [Internet]. bioRxiv; 2022 [cited 2024 Sep 20]. p.
660 2022.04.08.487609. Available from:
661 https://www.biorxiv.org/content/10.1101/2022.04.08.487609v1
662 59. Kosugi S, Hasebe M, Tomita M, Yanagawa H. Systematic identification of cell
663 cycle-dependent yeast nucleocytoplasmic shuttling proteins by prediction of
664 composite motifs. Proc Natl Acad Sci. 2009 Jun 23;106(25):10171–6.
665 60. Erdős G, Dosztányi Z. AIUPred: combining energy estimation with deep learning
666 for the enhanced prediction of protein disorder. Nucleic Acids Res. 2024 Jul
667 5;52(W1):W176–81.
668 61. Drozdetskiy A, Cole C, Procter J, Barton GJ. JPred4: a protein secondary structure
669 prediction server. Nucleic Acids Res. 2015 Jul 1;43(W1):W389–94.
670 62. Abramson J, Adler J, Dunger J, Evans R, Green T, Pritzel A, et al. Accurate
671 structure prediction of biomolecular interactions with AlphaFold 3. Nature. 2024
672 Jun;630(8016):493–500.
673 63. Fu L, Niu B, Zhu Z, Wu S, Li W. CD-HIT: accelerated for clustering the next-
674 generation sequencing data. Bioinformatics. 2012 Dec 1;28(23):3150–2.

675 64. Shen W, Le S, Li Y, Hu F. SeqKit: A Cross-Platform and Ultrafast Toolkit for
676 FASTA/Q File Manipulation. PLOS ONE. 2016 Oct 5;11(10):e0163962.
677 65. Steinegger M, Söding J. MMseqs2 enables sensitive protein sequence searching for
678 the analysis of massive data sets. Nat Biotechnol. 2017 Nov;35(11):1026–8.
679

680 **Figure legends**

681 **Fig. 1 Phylogenetic relationships of kolmioviruses.** The phylogenetic tree was inferred by the
682 Bayesian Markov chain Monte Carlo method based on an amino acid sequence alignment of DAg.
683 Posterior probabilities are shown for all nodes. Figure arts were created with BioRender.com or
684 downloaded from https://www.phylopic.org/. The scale bar indicates the number of amino acid
685 substitutions per site.

686

687 **Fig. 2 Phylogenetic analysis based on nucleotide sequences of complete scKoV genomes.** (**A**)
688 The phylogenetic tree was inferred by the maximum likelihood method using nucleotide
689 sequences of complete scKoV genomes. Bootstrap values are indicated at each branch. The
690 BioProjects of each SRA data that scKoV sequences originated are indicated with dark blue, blue,
691 light blue, and red circles, respectively. The scale bar indicates the number of nucleotide
692 substitutions per site. (**B**) Heat map of pairwise identities of scKoV variants based on nucleotide
693 sequences of complete genomes (lower left) and amino acid sequences of DAg (upper right). (**C**)
694 Detection of mixed infections with scKoV of different genogroups. For BioProject
695 PRJNA679636, their tissue of origin is indicated.

696

697 **Fig. 3 Genome organization and transcriptional pattern of scKoV.** (**A**) Self-
698 complementarities of scKoV. The predicted RNA structures were visualized using the Mfold web
699 server (56). (B) Genome organization of scKoV. Colored arrows indicate annotations (ORFs,
700 ribozymes, and poly-A signals). The numbers indicate nucleotide positions. (**C**) Predicted
701 genomic and antigenomic structures of scKoV. Gray numbers indicate nucleotide positions of
702 each predicted ribozyme. The names of secondary structural elements of ribozymes are indicated
703 in blue. Red triangles indicate catalytic sites. Information of SRR10526804 is indicated as a

704 representative. Information about other variants is provided in Figs. S2, S3, and S4. (**D**) Strand-
705 specific mapping coverage of original short reads of scKoV full-genome sequence. Colored
706 arrows indicate annotations (ORFs, ribozymes, poly-A signals). Light pink box indicates putative
707 intron. Green triangle indicates edge of the rod-like structure of circulated scKoV genome.
708 Information of SRR10526804 is indicated as a representative. Information about other variants is
709 provided in Fig. S5. (**E**) Secondary structures and expanded mapping patterns of the putative
710 promoter regions of scKoV. Conserved domains were annotated as previously reported (25). (**F**)
711 Nucleotide alignment of predicted intron region using representative variants of scKoV in each
712 genotype. Dots indicate common bases in the alignment. Gray and blue box indicate conserved
713 GU-AG boundary and polypyrimidine tract, respectively. Gray numbers indicate nucleotide
714 position in alignment of full-genome sequences.
715
716 **Fig. 4 Co-existing viruses in scKoV-positive RNA-seq data.** (**A**) Co-existing avian bornaviruses
717 (ABVs) (left panel) and scKoV-derived read number (right panel) detected from each RNA-seq
718 dataset are shown. Black indicates the presence of a viral contig, while white indicates its absence.
719 Read per million (RPM) of scKoV is shown as a heatmap. Results from RNA-seq data with
720 scKoV RPM $\geq$ 5 are shown. Full information is available in Fig. S8. (**B**) Scatter plot showing
721 RPM of scKoV and ABVs of each RNA-seq data. The linear prediction is shown as a dotted line.
722 The correlation coefficient (R^2) of the linear prediction is shown on the graph.
723

Table 1. Detection of scDeV reads in public RNA-seq data

Bio Project	SRA	Host				RPM (read per million)[a]	Tissue	full-length scDeV genome		
		Common name	Taxonomy					DDBJ accession	Length (bp)	GC content (%)
			Order	Family	Species					
PRJNA300534	SRR2915371[b]	Common canary	*Passeriformes*	*Fringillidae*	*Serinus canaria*	10.17	Skin	BR002460	1,672	54.7
PRJNA939570	SRR23747102					41.63	Fat tissue	BR002469	1,672	
	SRR23747110					96.01	Fat tissue	BR002470	1,674	
	SRR23747114					5.26	Fat tissue	BR002471	1,676	
	SRR23747122					57.30	Fat tissue	BR002472	1,672	
PRJNA591356	SRR10526804					758.69	Skin	BR002461[c]	1,672	54.5
	SRR10526806					570.30	Skin	BR002464[c]	1,672	54.6
	SRR10526807					525.41	Skin	BR002462	1,672	54.7
	SRR10526821					153.89	Skin	BR002465[c]	1,676	55.5
	SRR10526846					809.00	Skin	BR002461[c]	1,672	54.5
	SRR10526848					685.58	Skin	BR002464[c]	1,672	54.6
	SRR10526849					488.29	Skin			
	SRR10526851					194.19	Skin	BR002465[c]	1,676	55.5
	SRR10526845	European serin	*Passeriformes*	*Fringillidae*	*Serinus serinus*	5.52	Skin			
	SRR10526817	House finch	*Passeriformes*	*Fringillidae*	*Haemorhous mexicanus*	20.35	Skin			
	SRR10526824					16.80	Skin	BR002463	1,672	54.0
PRJNA679636	SRR13480239	Monk parakeet	*Psittaciformes*	*Psittacidae*	*Myiopsitta monachus*	16.38	Brain	BR002466	1,671	54.6
	SRR13480240					38.42	Brain	BR002467	1,671	54.6
	SRR13480246					22.48	Lung			
	SRR13480248					11.49	Ovary	BR002468	1,671	54.9

[a]This table only shows the SRA data wirh RPM > 5. The full version of the table is available as Supplementary Table S1.

[b]Identified in the previous study (Iwamoto et al. Virus Evol, 2021)

[c]Identical accession numbers indicate that the genome sequences obtained are identical.

Fig. 1

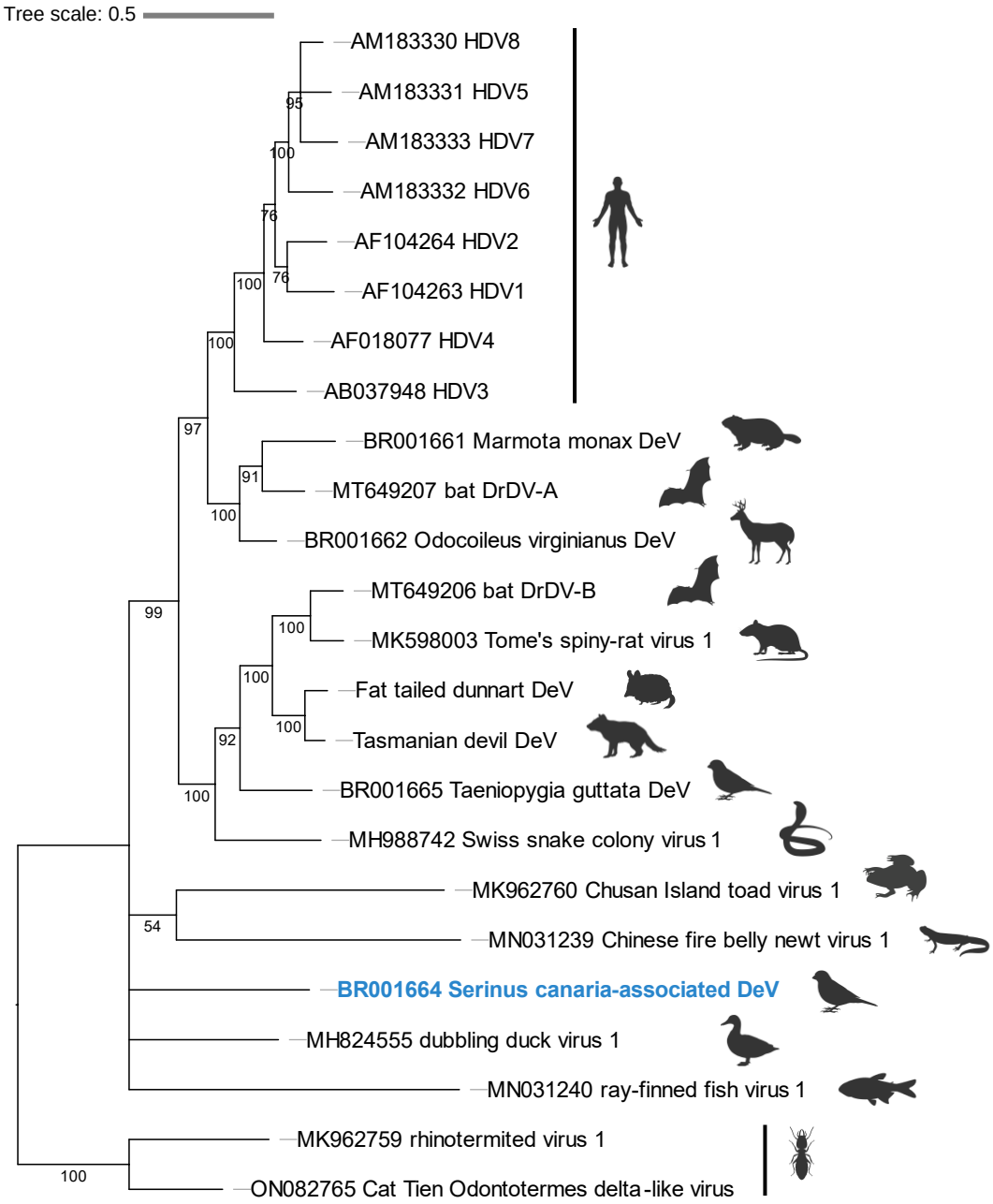
Tree scale: 0.5
AM183330 HDV8
AM183331 HDV5
AM183333 HDV7
AM183332 HDV6
AF104264 HDV2
AF104263 HDV1
AF018077 HDV4
AB037948 HDV3
BR001661 Marmota monax DeV
MT649207 bat DrDV-A
BR001662 Odocoileus virginianus DeV
MT649206 bat DrDV-B
MK598003 Tome's spiny-rat virus 1
Fat tailed dunnart DeV
Tasmanian devil DeV
BR001665 Taeniopygia guttata DeV
MH988742 Swiss snake colony virus 1
MK962760 Chusan Island toad virus 1
MN031239 Chinese fire belly newt virus 1
BR001664 Serinus canaria-associated DeV
MH824555 dubbling duck virus 1
MN031240 ray-finned fish virus 1
MK962759 rhinotermited virus 1
ON082765 Cat Tien Odontotermes delta-like virus
95
100
76
76
100
100
97
91
100
99
100
100
100
92
100
54
100

Fig. 2

(A)

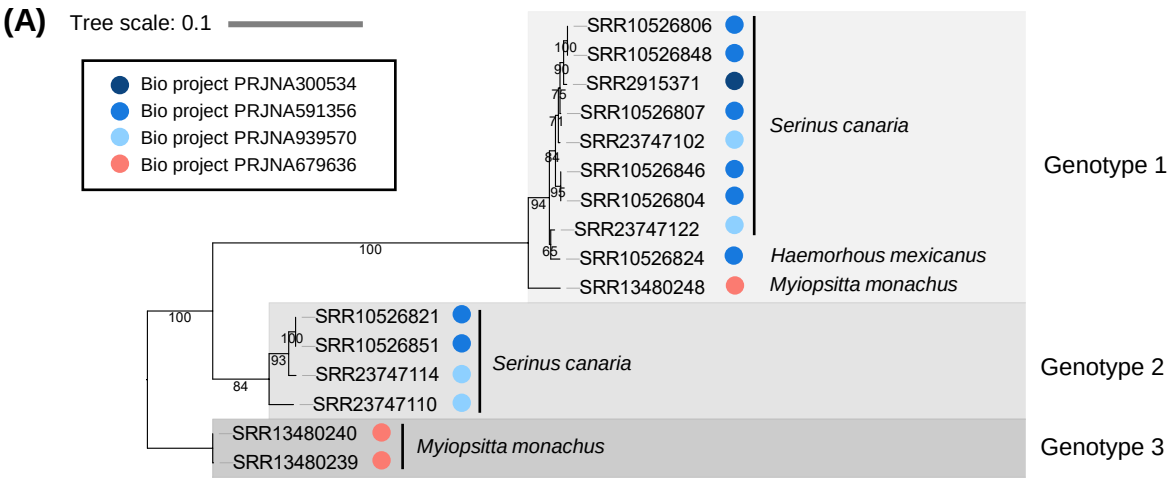

(B)

		1	2	3	4	5	6	7	8	9	10	11	12	13	14	15	16
1	SRR2915371 *S. canaria*		100.0	100.0	100.0	99.5	100.0	100.0	99.5	99.5	97.6	93.2	93.2	92.7	93.7	91.7	92.2
2	SRR10526806 *S. canaria*	99.5		100.0	100.0	99.5	100.0	100.0	99.5	99.5	97.6	93.2	93.2	92.7	93.7	91.7	92.2
3	SRR10526848 *S. canaria*	99.5	100.0		100.0	99.5	100.0	100.0	99.5	99.5	97.6	93.2	93.2	92.7	93.7	91.7	92.2
4	SRR10526807 *S. canaria*	99.5	99.4	99.4		99.5	100.0	100.0	99.5	99.5	97.6	93.2	93.2	92.7	93.7	91.7	92.2
5	SRR23747102 *S. canaria*	99.3	99.2	99.2	99.7		99.5	99.5	99.0	99.0	97.1	92.7	92.7	92.7	93.2	91.3	91.7
6	SRR10526804 *S. canaria*	99.2	99.2	99.2	99.2	99.3		100.0	99.5	99.5	97.6	93.2	93.2	92.7	93.7	91.7	92.2
7	SRR10526846 *S. canaria*	99.2	99.2	99.2	99.2	99.3	100.0		99.5	99.5	97.6	93.2	93.2	92.7	93.7	91.7	92.2
8	SRR10526824 *H. mexicanus*	98.3	98.3	98.3	98.6	98.7	98.4	98.4		100.0	98.1	92.7	92.7	92.2	93.2	91.3	91.7
9	SRR23747122 *S. canaria*	98.8	98.5	98.5	98.9	98.9	98.8	98.8	99.0		98.1	92.7	92.7	92.2	93.2	91.3	91.7
10	SRR13480248 *M. monachus*	95.6	95.3	95.3	95.6	95.6	95.9	95.9	95.6	95.9		92.2	92.2	91.7	92.7	90.8	91.3
11	SRR10526821 *S. canaria*	83.0	82.8	82.8	83.1	83.1	83.3	83.3	83.0	83.3	83.0		100.0	99.5	99.5	93.7	94.2
12	SRR10526851 *S. canaria*	83.0	82.8	82.8	83.1	83.1	83.3	83.3	83.0	83.3	83.0	100.0		99.5	99.5	93.7	94.2
13	SRR23747114 *S. canaria*	83.3	83.0	83.0	83.1	83.1	83.4	83.4	83.0	83.4	83.0	99.0	99.0		99.0	93.2	93.7
14	SRR23747110 *S. canaria*	83.4	83.3	83.3	83.5	83.6	83.8	83.8	83.1	83.6	83.1	96.5	96.5	96.4		94.2	94.7
15	SRR13480239 *M. monachus*	81.6	81.7	81.7	81.9	82.0	82.1	82.1	81.7	81.8	82.1	88.5	88.5	88.6	88.5		99.5
16	SRR13480240 *M. monachus*	81.7	81.7	81.7	82.0	82.0	82.2	82.2	81.8	81.9	82.1	88.5	88.5	88.6	88.5	99.9	

Identity (%)
High
Low
DAg (aa)
Genome (nt)

(C)

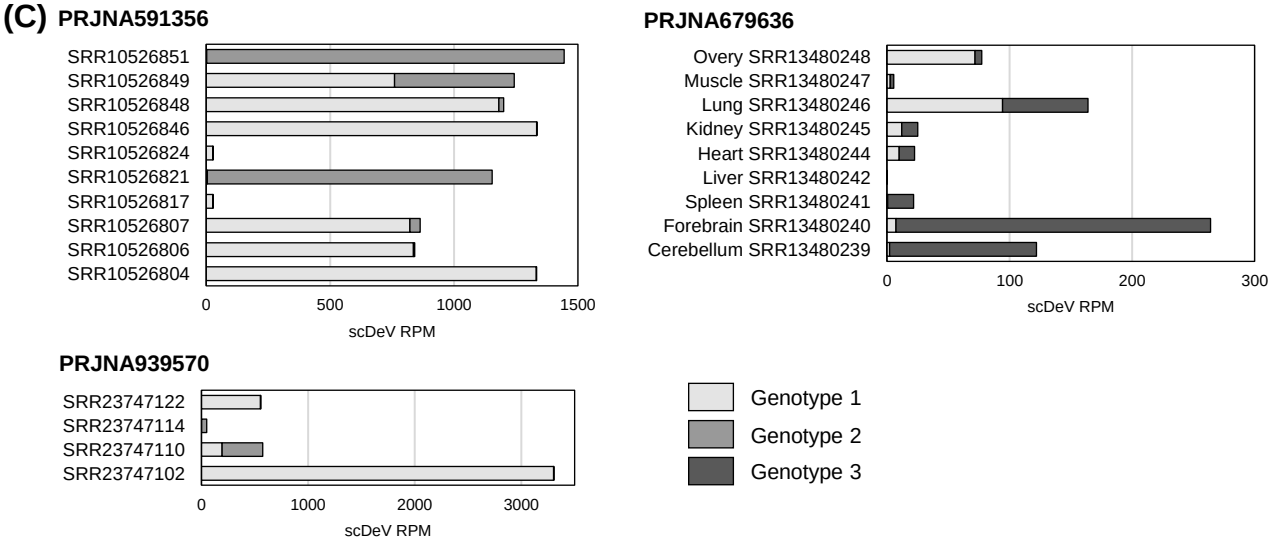

Fig. 3

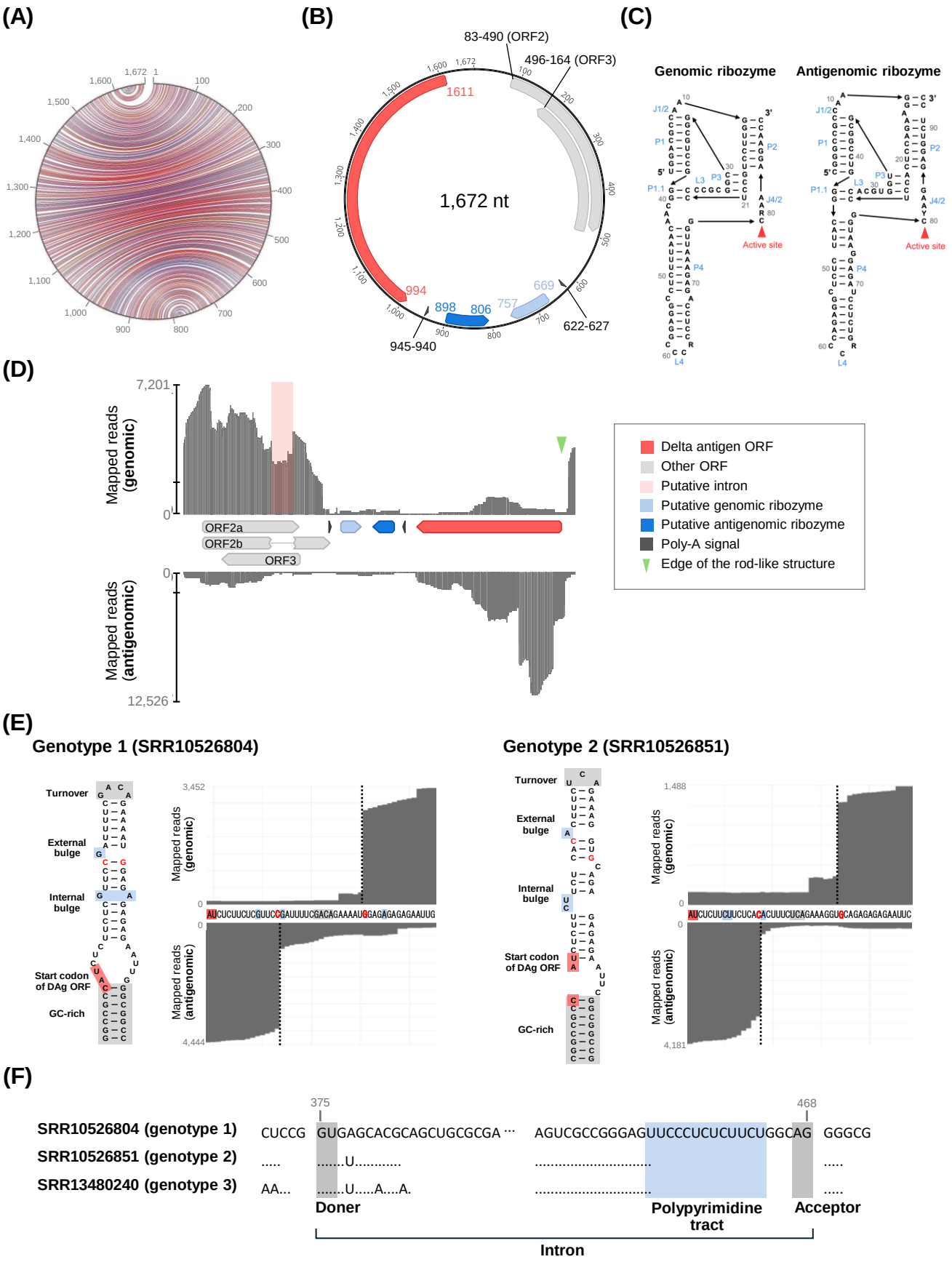
(A)
(B)
83-490 (ORF2)
496-164 (ORF3)
1611
1,672 nt
994
898
806
757
669
622-627
945-940
(C)
Genomic ribozyme
Antigenomic ribozyme
Active site
(D)
Mapped reads (genomic)
Mapped reads (antigenomic)
7,201
12,526
ORF2a
ORF2b
ORF3
Delta antigen ORF
Other ORF
Putative intron
Putative genomic ribozyme
Putative antigenomic ribozyme
Poly-A signal
Edge of the rod-like structure
(E)
Genotype 1 (SRR10526804)
Genotype 2 (SRR10526851)
Turnover
External bulge
Internal bulge
Start codon of DAg ORF
GC-rich
3,452
4,444
1,488
4,181
(F)
SRR10526804 (genotype 1)
SRR10526851 (genotype 2)
SRR13480240 (genotype 3)
375
468
CUCCG GUGAGCACGCAGCUGCGCGA ··· AGUCGCCGGGAGUUCCCUCUCUUCUGGCAG GGGCG
Doner
Polypyrimidine tract
Acceptor
Intron

Fig. 4

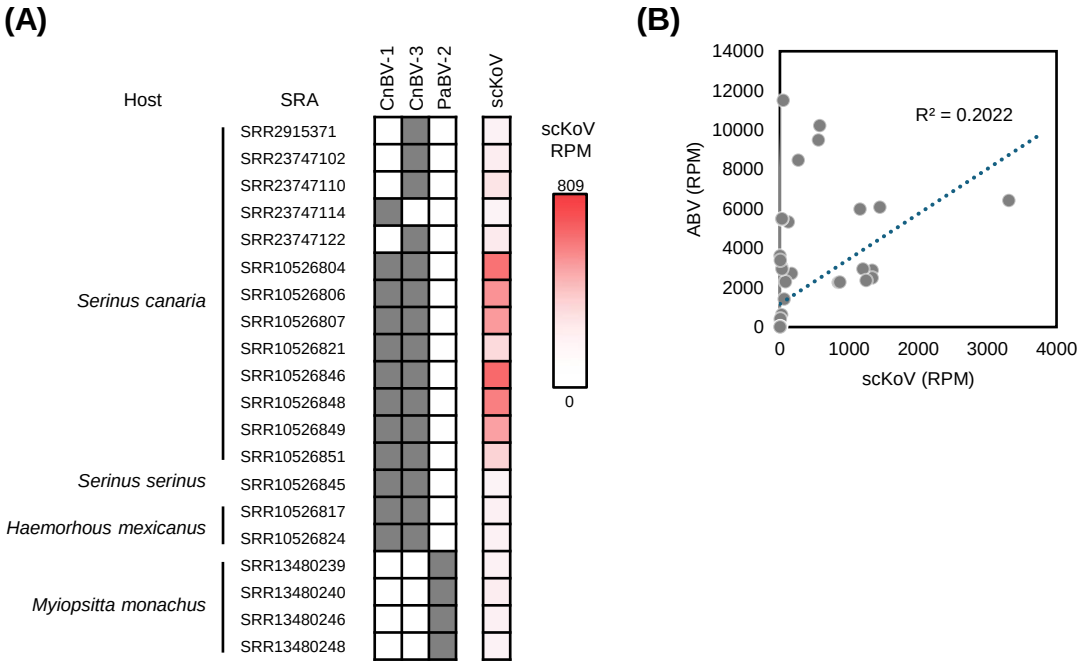
(A)
Host
SRA
CnBV-1
CnBV-3
PaBV-2
scKoV
scKoV RPM
809
0
Serinus canaria
SRR2915371
SRR23747102
SRR23747110
SRR23747114
SRR23747122
SRR10526804
SRR10526806
SRR10526807
SRR10526821
SRR10526846
SRR10526848
SRR10526849
SRR10526851
Serinus serinus
SRR10526845
Haemorhous mexicanus
SRR10526817
SRR10526824
Myiopsitta monachus
SRR13480239
SRR13480240
SRR13480246
SRR13480248
(B)
R² = 0.2022
ABV (RPM)
scKoV (RPM)
0
2000
4000
6000
8000
10000
12000
14000
0
1000
2000
3000
4000